Earthq Eng & Eng Vib (2018) 17: 235-250 **DOI**: https://doi.org/10.1007/s11803-018-0438-9

Analytical investigation of bidirectional ductile diaphragms in multi-span bridges

Xiaone Wei[1†] and Michel Bruneau[2‡]

1. *Michael Baker International, Chicago, IL 60606, USA*

2. *Department of Civil, Structural, and Environmental Engineering, University at Buffalo, Buffalo, NY 14260, USA*

Abstract: In the AASHTO Guide Specifications for Seismic Bridge Design Provisions, ductile diaphragms are identified as Permissible Earthquake-Resisting Elements (EREs), designed to help resist seismic loads applied in the transverse direction of bridges. When adding longitudinal ductile diaphragms, a bidirectional ductile diaphragm system is created that can address seismic excitations acting along both the bridge's longitudinal and transverse axes. This paper investigates bidirectional ductile diaphragms with Buckling Restrained Braces (BRBs) in straight multi-span bridge with simply supported floating spans. The flexibility of the substructures in the transverse and longitudinal direction of the bridge is considered. Design procedures for the bidirectional ductile diaphragms are first proposed. An analytical model of the example bridge with bidirectional ductile diaphragms, designed based on the proposed methodology, is then built in SAP2000. Pushover and nonlinear time history analyses are performed on the bridge model, and corresponding results are presented. The effect of changing the longitudinal stiffness of the bidirectional ductile diaphragms in the end spans connecting to the abutment is also investigated, in order to better understand the impact on the bridge's dynamic performance.

Keywords: bidirectional ductile diaphragm, seismic resistance, multi-span bridge with floating spans

1 Introduction

The ductile end diaphragm concept was originally introduced for steel bridges to reduce their seismic vulnerability, and research has been conducted analytically and experimentally to study how this concept improves the bridges' seismic performance in their transverse direction (Zahrai and Bruneau, 1998, 1999a, 1999b; Sarraf and Bruneau,1998a, 1998b). Based on those findings, design procedures were proposed in Bruneau *et al*. (2002) for specially detailed transverse ductile end diaphragms in slab-on-girder and deck-truss bridges, using energy dissipation devices such as shear links, Triangular-plate Added Damping and Stiffness Devices (TADAS), or Eccentric Braced Frame (EBF). Carden *et al.* (2006a, 2006b) tested a straight single-span two-girder bridge model with ductile end diaphragms using single angle X braces and Buckling Restrained Braces (BRBs). Both types of end diaphragms showed satisfactory ductile responses in the bridge models under reversed static loads and the 1940 El Centro earthquake ground motion. Provisions for using specially detailed transverse ductile end diaphragms in steel bridges were later introduced in the AASHTO Guide Specifications for LRFD Seismic Bridge Design (2011) as Permissible Earthquake-Resisting Elements (EREs). Subsequently, Celik and Bruneau (2011) extended the concept of transverse ductile end diaphragms to bidirectional End Diaphragm System in straight or skew slab-on-girder bridge superstructures, to resist bidirectional earthquake excitations. BRBs were used in the two proposed schemes in a single span bridge as shown in Fig.1, to provide ductile responses to all horizontal seismic forces. A bridge with floating span was considered in this case, and the bridge's deck was supported on bidirectional sliding bearings or other bearings with negligible strength to horizontal deformations at the abutment. Static pushover analyses were performed on the bridge model with both ductile diaphragm system configurations. Effect of changing parameters of the ductile end diaphragm systems such as stiffness, yield strength, yield displacement as a function of a given design ductility level, were investigated in bridges with varying skew angles. Dynamic inelastic responses of these two ductile diaphragm system schemes were studied in Wei and Bruneau (2017), by subjecting bridge models with various skewness to actual earthquake excitations in the parametric nonlinear time history analyses. From

Correspondence to: Xiaone Wei, Michael Baker International, Chicago, IL 60606, USA
E-mail: xiaonewe@buffalo.edu
†Civil Associate; ‡Professor

Received January 20, 2018; **Accepted** March 1, 2018

those analytical results, seismic end displacement demands of the BRBs were obtained to design the BRBs to ensure the desired ductile bidirectional performance of the ductile diaphragm systems. Since the resulting displacement demands for the BRBs required larger out-of-plane displacement capacity than any BRB ever tested, quasi-static experiments were conducted in Wei and Bruneau (2018), by applying a regime of relative end displacements demands to the BRBs, to investigate if specially designed BRBs' end connections could sustain the required displacement demands when installed in ductile diaphragm systems. Test results of the BRB specimens showed no undesirable end-plate failure or instability. A recommended design procedure for the ductile diaphragm systems with BRBs in both straight and skew bridges was developed. Note that the concept of bidirectional ductile diaphragm systems was only contemplated in the context of single span bridges with floating superstructures as mentioned above. When implemented in multi-span bridges, the bidirectional ductile diaphragm systems are connected to bridge bents between spans. Therefore, the seismic behavior and response of the bidirectional ductile diaphragm system are affected by the stiffness of the substructure. The bidirectional diaphragm systems need to be designed to ensure that the substructures remain elastic during the earthquakes.

This paper investigates the bidirectional ductile diaphragm system of the first configuration in Fig.1 by implementing it in a straight multi-span bridge with simply-supported floating spans. The flexibility of the substructures in the transverse and longitudinal direction of the bridge are considered when designing bidirectional ductile end diaphragms. The design concept of the bidirectional ductile diaphragms in the multi-span bridge is first proposed. An analytical model of the example bridge with the designed bidirectional ductile diaphragm systems is then built in *SAP2000 Version 16*. Pushover and nonlinear time history analyses are performed on the bridge model, and corresponding results are presented. The effect of changing the longitudinal stiffness of the bidirectional ductile diaphragm systems in the end spans connecting to the abutment is also investigated, in order to better understand the impact on the bridge's seismic performance.

2 Design concept

Figure 2a shows a typical straight simply-supported bridge with three floating spans. The bidirectional ductile End Diaphragm System (EDS) is located on top of the abutments at the two end spans. The bidirectional ductile Intermediate Diaphragm System (IDS) is located on top of the bents for the end and middle spans. Note that there are two IDSs on top of each bent. Schematic views of the resulting ductile diaphragms showing the BRBs in the transverse and longitudinal direction are illustrated in Fig. 2b and 2c respectively. The transverse BRBs in Fig. 2b were implemented between the steel girders, and the BRBs can be pin-connected to the web stiffeners of the girders (which are not shown in Fig. 2b). Fig. 2c shows the longitudinal BRBs connected between the cap beams of the bent or the abutment to

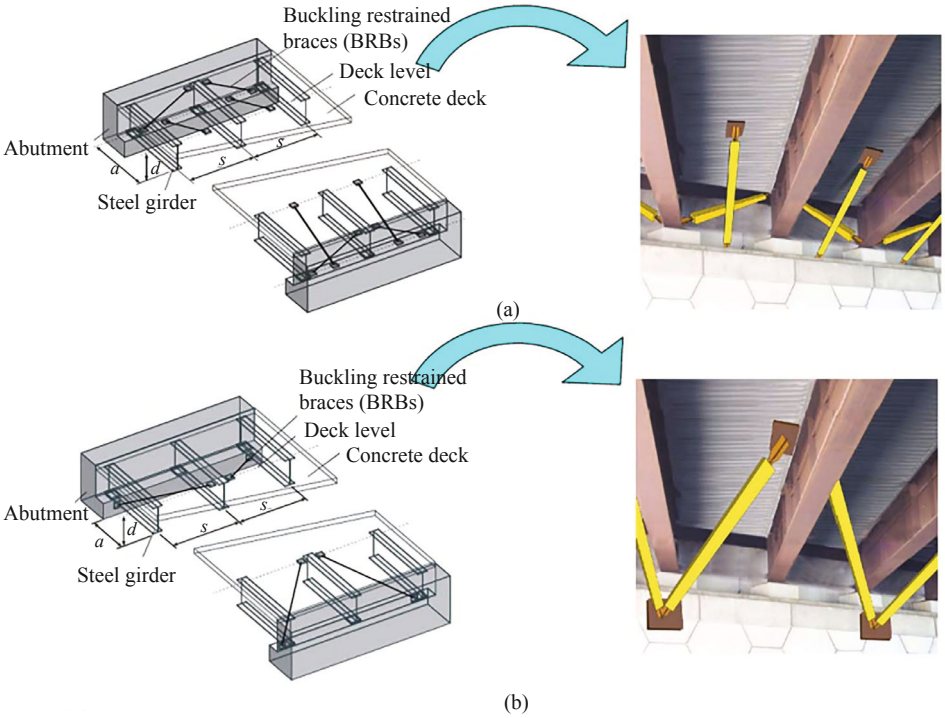

Fig. 1 Proposed Schemes for Bridge Ductile End Diaphragms: (a) EDS-1; (b) EDS-2 (adapted from Celik and Bruneau, 2007)

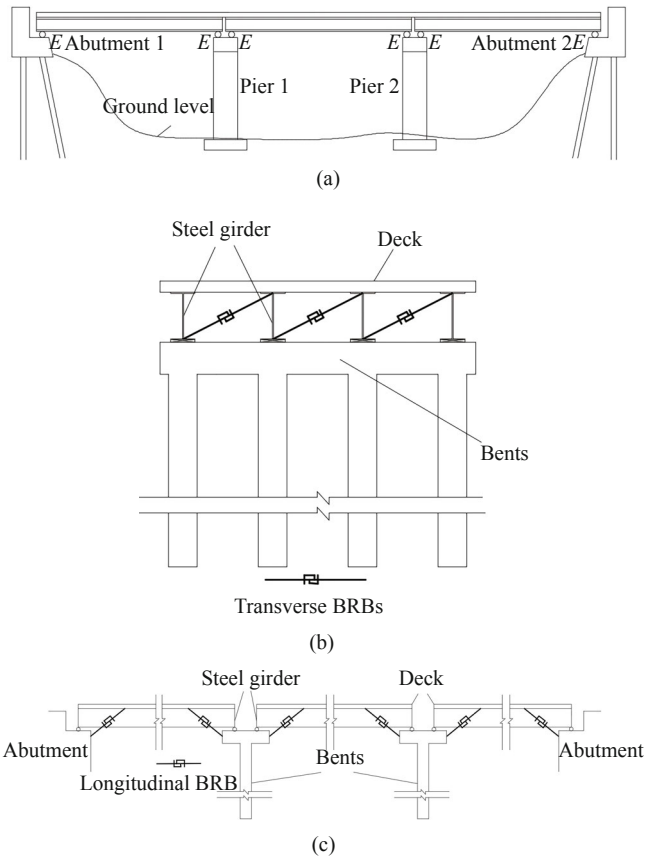

Fig. 2 Illustration of BRBs in bidirectional ductile diaphragms in a three-span bridge: (a) bridge overview; (b) transverse direction; (c) longitudinal direction

the top of the steel girders (i.e. bottom of the concrete slab). For both orientations, alternative configurations are possible (Wei and Bruneau, 2016). Note that the numbers of BRBs used in Fig. 2b can change based on different bridge configurations and strength/stiffness demand provided by the BRBs.

The design of the bidirectional ductile diaphragms in multi-span bridges needs to consider the strength and stiffness contribution of the bridge bents in both the longitudinal and transvers directions. Figure 3 illustrates the response of a three-span bridge with bidirectional ductile diaphragms in the transverse and longitudinal directions, when subjected to horizontal ground motions during earthquakes. In both figures, the solid and dashed lines represent the undeformed and deformed shape of the bridge, respectively. The design intent is to keep the substructures elastic under the seismic loads during earthquakes. The BRBs in the bidirectional ductile diaphragms are designed to yield and deform inelastically, in order to absorb and dissipate the energy and keep the rest of the structure elastic during the earthquake.

In the design procedure outlined below, the mass of each bridge span is *M*. The span length is *L*. The superstructure's moment of inertia is, *I*, which considers the slab and girders acting as a unit about a vertical axis perpendicular to the deck in the transverse direction. The bent stiffness in the transverse and longitudinal direction are K_{bt} and K_{bl}, respectively. The transverse and longitudinal stiffness of the bidirectional ductile diaphragm system at each end of the span are K_{dt} and K_{dl}, respectively. The stiffness of the girder stiffeners in the bridge's transverse direction is K_g, which is the total stiffness of the web bearing stiffeners of all girders.

3 Bridge behavior in transverse direction

The two end spans of the bridge are supported on an abutment at one of their end, and a bridge bent at their other end. The middle span of the bridge is supported on a bridge bent at both of its ends. Comparing the three spans, the behavior of the bridge in the transverse direction is expected to be affected by the flexibility of the bridge bent (substructure) more at the middle span than at the end spans. Therefore, the transverse diaphragms with BRBs in the middle span were first designed. For the purpose of modeling transverse response, the middle span of the bridge with transverse ductile diaphragms at both ends can be simplified as a beam with length *L*, uniform mass, *M/L*, and uniform stiffness, *EI*, supported on elastic spring groups as shown in Fig. 4. Since each bent supports two adjacent spans, the stiffness K_{et} in Fig. 4 is not the entire transverse stiffness of the bridge

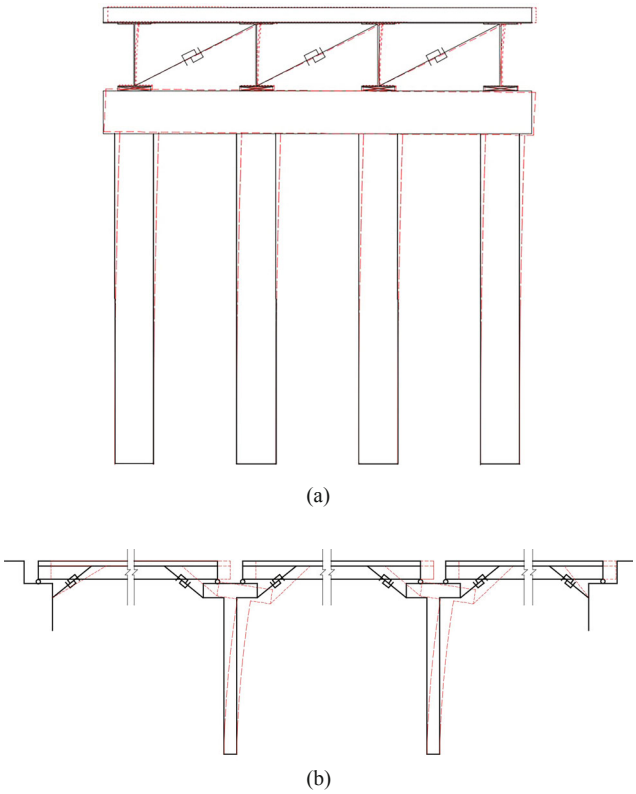

Fig. 3 Illustration of dynamic responses of a multi-span bridge in: (a) transverse direction; (b) longitudinal direction

bent, K_{bt}. As a simplification, K_{et} is assumed to be half of K_{bt}, here. However, note that compared with the bent, the abutment supporting the end spans has much larger stiffness, and this can impact the ratio of K_{et}/K_{bt} for the middle span (i.e., its value can be a function of the transverse bent stiffness K_{bt}).

The beam in Fig.4 can be viewed as simply-supported at its ends by springs with elastic stiffness, K_{nt}, which is:

$$K_{nt} = \frac{1}{\frac{1}{K_{et}} + \frac{1}{K_g + K_{dt}}} \tag{1}$$

where $K_{et} = 0.5K_{bt}$.

Alfawakhiri and Bruneau (2001) provided Equations (2) to (5), which indicate the dynamic parameters for the first mode of the beam model shown in Fig. 5. The shape function for this first mode is:

$$\varphi_1(x) = \frac{3.2(xL^3 - 2x^3L + x^4 + 12BL^4)}{L^4(1 + 38.4B)} \tag{2}$$

where the factor B is:

$$B = \frac{\frac{EI}{L^3}}{K_{nt}} \tag{3}$$

The period of the first mode is:

$$T_1 = 2\pi\sqrt{\frac{M(30B^2 + B + 31/3024)}{K_{nt}B(60B + 1)}} \tag{4}$$

The generalized mass is:

$$M_1^* = \frac{M(60B + 1)^2}{60(60B^2 + 2B + 31/1512)} \tag{5}$$

The spectral displacement of the corresponding SDOF system of the transverse beam model in Fig. 4 is:

$$\delta_{ut} = \frac{V_{sat}}{M_1^*\omega_1^2} = \frac{MS_{at}}{M_1^*\omega_1^2} = \frac{MS_{at}T_1^2}{M_1^* 4\pi^2} \tag{6}$$

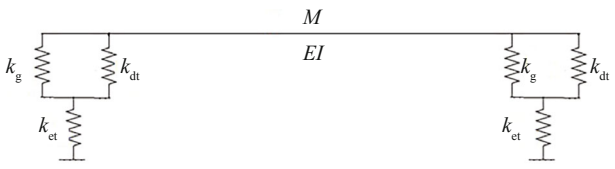

Fig. 4 Simply supported transverse beam model on elastic springs

where V_{sat} is the elastic force demand based on the spectral acceleration, S_{at}, corresponding to the period T_1.

The yield strength of the spring group at one end is V_{yt}, which is designed to correspond to the yielding of the BRBs in the transverse ductile diaphragms. When the yield forces are reached in the transverse BRBs in the ductile diaphragm, the girder bearing stiffeners and the columns should remain elastic. And the yield displacement of the spring group, δ_{yt}, is:

$$\delta_{yt} = \frac{V_{yt}}{K_n} \tag{7}$$

The ductility of the spring group, μ_{dt}, is

$$\mu_{dt} = \frac{\delta_{ut}}{\delta_{yt}} \tag{8}$$

The ductility of the beam system, μ_e, is defined as the ratio of the maximum displacements, δ_{ut}, at the center of the beam over the displacement of the spring group, which corresponds to the yielding of the spring system, δ_{yt}. The relationship between the ductility of the beam system and the spring group is given in Eqs. (9)–(11) below provided by Alfawakhiri and Bruneau (2001):

$$\mu_e = 1 + \frac{\mu_{dt} - 1}{\varphi_1(0)\Gamma_1} \tag{9}$$

where:

$$\varphi_1(0) = \frac{38.4BL^4}{L^4(1 + 38.4B)} \tag{10}$$

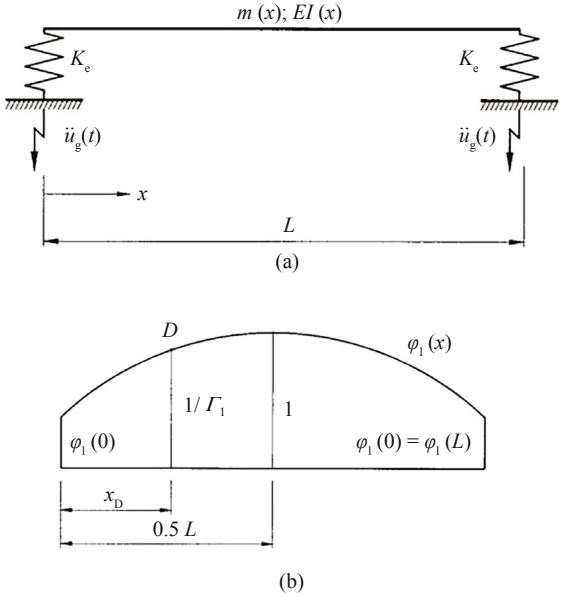

Fig. 5 (a) Simply supported transverse beam model on elastic springs; (b) first mode shape (Alfawakhiri and Bruneau, 2001)

$$\Gamma_1 = \frac{(1+38.4B)(60B+1)}{38.4(60B^2+2B+31/1512)} \tag{11}$$

Based on the displacement and force relationship in the individual spring in the spring group, the local ductility of the individual transverse BRB is derived as:

$$\mu_{BT} = \mu_{dt}(1+\frac{K_{dt}+K_g}{K_{et}}) - \frac{K_{dt}+K_g}{K_{et}} \tag{12}$$

Given the assumed stiffness, K_{dt} , and yield strength, δ_{yt} , of the transverse diaphragm, the acceptable design parameters and ductility of the individual BRB, such as its yield displacement and yield strength, can also be determined by trial and error using the above Equations, based on the configurations of the transverse BRBs in the transverse ductile diaphragms.

4 Bridge behavior in longitudinal direction

Similar to the bridge beam model of the middle span in the transverse direction, the middle span with longitudinal diaphragms at both ends can also be simplified as a beam supported on spring groups as shown in Fig. 6. The stiffness K_{el}, representing the stiffness contribution from the bridge bent in the longitudinal direction, is also only a portion of the entire bent's longitudinal stiffness, K_{bl}. Here, the ratio between K_{el} and K_{bl} is assumed to be 0.5, which is also subjected to change for different longitudinal bent stiffness K_{bl}.

The total stiffness of the spring group at each end, K_{nl}, in Fig. 6 can be expressed as:

$$K_{nl} = \frac{1}{\frac{1}{K_{el}}+\frac{1}{K_{dl}}} \tag{13}$$

where $K_{el} = 0.5K_{bl}$

The period of the vibration mode in the longitudinal direction is:

$$T_2 = 2\pi\sqrt{\frac{M}{2K_{nl}}} \tag{14}$$

The spectral displacement of the corresponding SDOF system of the longitudinal beam model in Fig. 6 is:

$$\delta_{ul} = \frac{V_{sal}}{M\omega_2^2} = \frac{MS_{aL}}{M\omega_2^2} = \frac{S_{aL}T_2^2}{4\pi^2} \tag{15}$$

Fig. 6 Simply supported longitudinal beam model on elastic springs

where V_{sal} is the elastic force demand based on the spectral acceleration, S_{aL}, corresponding to the period T_2.

The yield strength of the spring group at one end is V_{yl}, which is designed to correspond to the yielding of the BRBs in the longitudinal ductile diaphragms. When the yield force is reached in the longitudinal BRBs, the column remains elastic. The corresponding yield displacement of the spring group, δ_{yl} , is:

$$\delta_{yl} = \frac{V_{yl}}{K_{nl}} \tag{16}$$

The ductility of the spring group, μ_{dl}, is

$$\mu_{dl} = \frac{\delta_{ul}}{\delta_{yl}} \tag{17}$$

The ductility of the spring group is the same as the ductility of the beam system in Fig. 6. The local ductility of the individual longitudinal BRB is derived as:

$$\mu_{BL} = \mu_{dl}(1+\frac{K_{dl}}{K_{el}}) - \frac{K_{dl}}{K_{el}} \tag{18}$$

Similar to the transverse BRBs in the bidirectional ductile diaphragms, the acceptable design parameters and ductility of the longitudinal BRB can be determined by trial and error.

5 Design of bidirectional ductile diaphragm systems in an example multi-span bridge

An example multi-span bridge, taken from Zahrai and Bruneau (1999a), has three 40 m (131 ft) long spans. Each span is simply-supported on the reinforced concrete bents, which have four columns of 0.9 m (35.4 in) diameter and 5 m (16.4 ft) height. The mass of the bridge in each span is 286 kg (630 lbs). Four WWF47×224 steel girders were used with a girder-to-girder spacing of 2 m (78.75 in). The location of the bridge was chosen at Memphis, TN with latitude 35.15ºN, and longitude 90.17ºW. The site soil is class C. The target response spectrum in Fig. 7 was obtained from USGS (2017) with the 2017 USGS National Hazard Map for a 7% probability of being exceeded in 75 years (or 975 years return period). The damping ratio considered in this design spectrum is 5% of the critical damping. The following are the spectral response acceleration parameters: S_{ds} = 0.74 g and S_{d1} = 0.365 g.

The middle span in this multi-span bridge was first used to determine the design parameters of the BRBs in the bidirectional ductile diaphragms at its two ends. The bidirectional ductile diaphragms are designed to have the same yield strength and stiffness in both directions. The designs calculation are not described here due to space constraints (details are presented in Wei and Bruneau, 2016). The stiffness of the ductile diaphragm is 8.75×10^4

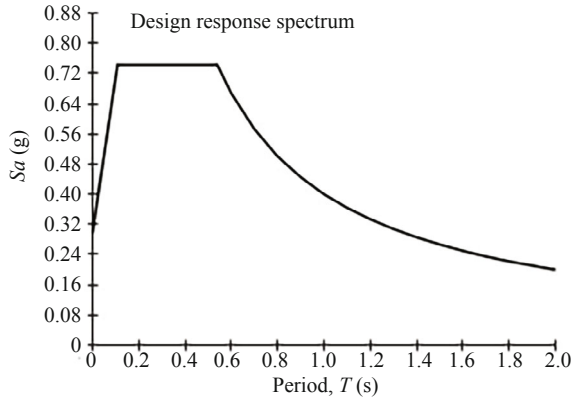

Fig. 7 Design response spectrum from Memphis, TN

kN/m (500 kip/in) in both the transverse and longitudinal directions. The yield displacement of the ductile diaphragm (i.e. the relative displacement between its top and bottom) is 2.6 mm (0.102″), when the BRBs yield. The stiffeners at the end of each girder were made from two plates placed at each side of the girder's web. The original stiffener plates from the bridge example were used here, and each has a height of 1.2 m (47.25″), width of 0.1 m (3.93″) and thickness of 10 mm (0.395″). The total transverse stiffness provided by all the stiffeners at the end of the girders is 1.2×10^4 kN/m (68.5 kip/in). The entire bridge bents' stiffness K_{bt} and K_{bl} are 3×10^5 and 7.5×10^4 kN/m (1713 and 428 kip/in) in the transverse and longitudinal direction, respectively. Note that the longitudinal stiffness of the bent is only 1/4 of that in the transverse direction. By adding the displacement of the bridge bent, the transverse and longitudinal displacements of the middle span at both ends δ_{yt} and δ_{yl}, where the bidirectional ductile diaphragm is located, are 4.32 mm (0.170″) and 8.66 mm (0.341″), when the transverse and longitudinal BRBs yield, respectively. Two transverse BRBs and one longitudinal BRB were used in the bidirectional ductile diaphragm at one end of the bridge's middle span. The steel material used in the BRB core plate is assumed to be A500 Gr. B with yield strength of 317 MPa (46 ksi). The inclination angle of the transverse BRB is 31 degrees from the deck, which is dependent on the girder height and spacing. The length of the transverse BRB is 2.33 m (91.8″). The yield length ratio of the transverse BRBs is 0.6. The cross sectional area of the yield core in the transverse BRB is 420 mm^2 (0.65 in^2), resulting in a yield force of 133.5 kN (30 kips). The axial yield displacement of the transverse BRB is 2.2 mm (0.087″). The longitudinal BRB has a length of 1.56 m (61.5 in), with an inclination angle of 50.2 degrees from the deck. The yield length ratio of the longitudinal BRBs is 0.67. The cross sectional area of the yield core in the longitudinal BRB is 1122 mm^2 (1.74 in^2), resulting in a yield force of 356 kN (80 kips). The axial yield displacement of the longitudinal BRB is 1.67 mm (0.066″). The pairs of girder stiffeners at each end of the individual girders have the lateral yield strength of 22 kN (5 kips) and yield displacement of 7.5 mm (0.293″). Note that the specific details of the BRBs can be designed differently as long as the stiffness and strength provided by them are the same as for the BRB designs used here.

The isolated middle span supported on the bridge bent has the resulting periods of 0.333 and 0.464 s in the transverse and longitudinal direction, respectively. Note that half of the bridge bents' stiffness in both the transverse and longitudinal direction was used for the middle span's bridge bent. Both periods fall on the plateau of the design response spectrum in Fig. 7. The spectral displacement δ_{ut} in the transverse direction is 21 mm (0.827″), which result in the ductility μ_{dt} of 4.86 in the transverse spring group. The bridge's transverse displacement ductility μ_e at the middle of the span is 5.4, and the corresponding transverse BRB ductility μ_{BT} is 7.2. The spectral displacement δ_{ul} in the longitudinal direction is 39 mm (1.535″), which results in the longitudinal displacement ductility μ_{dl} of 4.56. The corresponding longitudinal BRB ductility μ_{BL} is 12.8.

Note that, for the above simple spectral analyses, the bidirectional ductile diaphragms were only designed for the middle spans. Therefore, in the initial analyses of the more explicit three-span bridge model that follows, the end spans use the same BRBs in their bidirectional ductile diaphragms as the middle span, and the dynamic behavior of the bridge is accessed for that condition. The theoretical displacement demands and ductilities calculated above are then compared below with the values obtained from the nonlinear time history analyses and adjustments are made as deemed necessary.

6 SAP2000 bridge model

The above designed bridge is modeled as a three-dimensional spine structure with line elements, representing the slab and girders in the superstructure. The EDSs and IDSs are numbered as shown in Fig. 8a. Figure 8b shows the enlarged view of EDS-1 on top Abutment-1 at the left end of Span1. EDS-2 on top of Abutment-2 at the right end of span 2 is the mirror image of EDS-1. The longitudinal BRB, i.e. BRBL1, was built horizontally in line with the girder in both EDSs. This horizontal longitudinal BRB still provides the same stiffness and strength to the bridge structures as the inclined longitudinal BRBs in Fig. 2c in the longitudinal direction. There are three open spaces between the four girders in Fig. 8b, and the three inclined girder stiffener links installed there, i.e. G-1 to G-3, were modeled to represent the four girder end stiffeners at the end of Span-1. In other words, the added lateral/transverse stiffness and strength of links G1-G3 is equivalent to that of the four girder end stiffeners. Two transverse BRBs, i.e. BRB-T-1 and BRB-T-2, were placed parallel to the girder stiffener links G-1 and G-3 as shown in Fig. 8b.

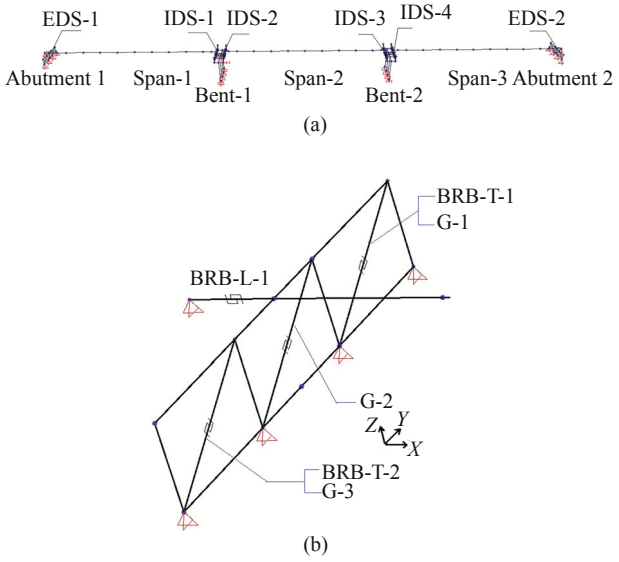

Fig. 8 (a) SAP2000 model of the multi-span bridge (b) enlarged view of the EDS-1 on top of Abutment-1

Figure 9a shows the enlarged view of IDS-2 and IDS-3 (in Fig. 8a) on top of Bent-1. Similarly, IDS-3 and IDS-4 on top of Bent-2 are the mirror image of IDS-1 and IDS-2 on top of Bent-1. The transverse ductile diaphragms in IDS-1 and IDS-2 are separated, so that the longitudinal BRBs can be modeled connecting the superstructure spine line to the bridge bents. The spacing between the two ductile diaphragms on top of the bent was built the same as the girder spacing. Therefore, the longitudinal BRBs in IDS-1 and IDS-2, i.e. BRB-L-2 and BRB-L-3, have an inclination angle of 50.2 degrees from the deck, which is the same as the design inclination angle of the longitudinal BRBs designed in Fig. 3. The IDSs have the same transverse BRBs and girder stiffener links layout as the EDSs. Figure 9b shows the enlarged side view the IDS-1 with columns in Bent-1.

The line element in Fig. 8a representing the superstructure (deck and girders) was defined with uniform mass, *M/L*, and uniform stiffness, *EI*. The BRBs and girder stiffener links were modeled as bilinear links using the Wen Plasticity property, as defined in *SAP2000* reference manual (2016). The columns in Fig. 9b were modeled as frame elements and divided in four segments. Fiber P-M2-M3 hinges were used at the ends of each segment. Each fiber hinge length was set as 10% of the length of the member. The rest of the lines representing elements in Figs. 8 and 9 were modeled as rigid elements to complete the structure.

The BRBs and girder stiffener links are numbered from left to right as shown in Figs. 8 and 9. Table 1 categorized the BRBs and the girder stiffener links in groups, which had the same response. The BRBs in the column named "representative member" are picked from the group with the same responses, and they will be used in the following sections for explaining the analyses results. Table 2 shows a summary of the properties used for the BRBs and girder stiffener links in the bridge model.

7 Pushover and nonlinear time history analyses

Pushover analyses were first performed on the *SAP2000* bridge model in the longitudinal and transverse directions, respectively. Displacement control was used using a control displacement at the middle of the bridge (i.e. middle of Span-2). Point loads were applied to the bridge at the level of the bridge deck along the bridge in both directions. The resulting pushover curves of the bridge model are shown in Fig.10 for the longitudinal and transverse direction, respectively. The first and second stiffness change points in Fig. 10a, corresponding to the longitudinal displacement of 3.91 mm (0.154″) and 14.27 mm (0.562″) at the middle of Span-2, indicate

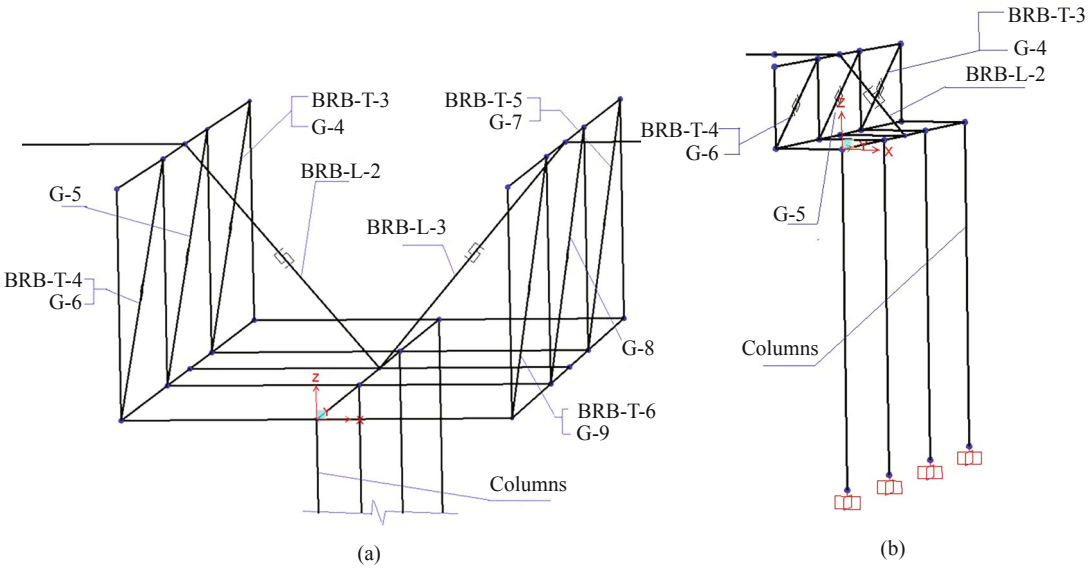

Fig. 9 Enlarged view of the IDS-1 and IDS-2 on top of Bent-1 (a) top view (b) half side view

Table 1 List of BRBs and girder stiffener links in the SAP2000 model

	Representative Member	Location	BRBs with the same response (Location of BRBs)
Longitudinal BRB	BRB-L-1	EDS-1	BRB-L-6 (EDS-2)
	BRB-L-2	IDS-1	BRB-L-5 (IDS-4)
	BRB-L-3	IDS-2	BRB-L-4 (IDS-3)
Transverse BRB	BRB-T-1	EDS-1	BRB-T-2 (EDS-1); BRB-T-11,12 (EDS-2)
	BRB-T-3	IDS-1	BRB-T-4 (IDS-1); BRB-T-9,10 (IDS-4)
	BRB-T-5	IDS-2	BRB-T-6 (IDS-2); BRB-T-7,8 (IDS-3)
Girder stiffeners	G-1	EDS-1	G-2,3 (EDS-1); G-16,17,18 (EDS-2)
	G-4	IDS-1	G-5,6 (IDS-1); G-13,14,15 (IDS-4)
	G-7	IDS-2	G-8,9 (IDS-2); G-10,11,12 (IDS-3)

Table 2 BRBs and girder links summary in the SAP2000 bridge model

	Longitudinal BRB		Transverse BRBs	Girder stiffener links
	horizontal	inclined		
Numbers	2	4	12	18
Yield strength (kN)	227	354	132	34.7
Yield displacement (mm)	2.59	1.68	2.21	6.38

that the longitudinal BRBs in the EDS and IDS yielded, respectively. The first and second stiffness change points in Fig. 10b, corresponding to the transverse displacement of 4.8 mm (0.189″) and 10.1 (0.398″) at the middle of Span-2, indicate that the transverse BRBs and girder stiffener links yielded, respectively.

Pushover analyses were also performed on the individual bent with four columns in the longitudinal and transverse directions. The yield displacements at the top of the bents are 23 mm (0.906″) and 13.26 mm (0.522″) in the longitudinal and transverse directions, respectively, when the hinge at the bottom of the columns indicated yielding.

For the time-history analyses, seven pairs of ground motions, shown in Fig.11, were arbitrarily selected from the 44 pairs of ground motions specified in FEMAP695 (2009). Although the ground motions recommended by FEMA-P695 were developed for studies on building structures, this set of ground motions is considered adequate and having the broad variability necessary to investigate the displacement responses of the bridge with BRBs in the bidirectional ductile end diaphragms. Each pair of ground motions have different duration and time steps. The name for each of the two ground motions in a pair, "GM-*i*-*j*", indicates that the *j*-th ground motion in the *i*-th pair.

The first and second periods of the bridge model are 0.41 and 0.307 s, which correspond to the bridge's longitudinal and transverse direction, respectively. At both of these two periods, the response spectrum of the 14 ground motions (i.e. 7 pairs) do not match the design response spectrum in Fig. 7. Therefore, each ground motion was scaled in order to have the same spectral acceleration as the design response spectrum at

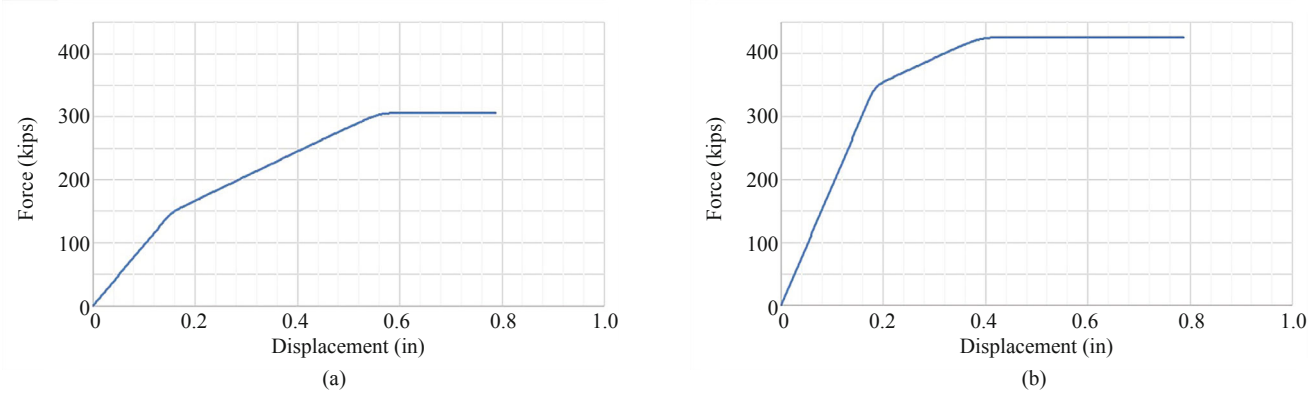

Fig. 10 Pushover curves of the multi-span bridge model in the: (a) longitudinal direction; (b) transverse direction

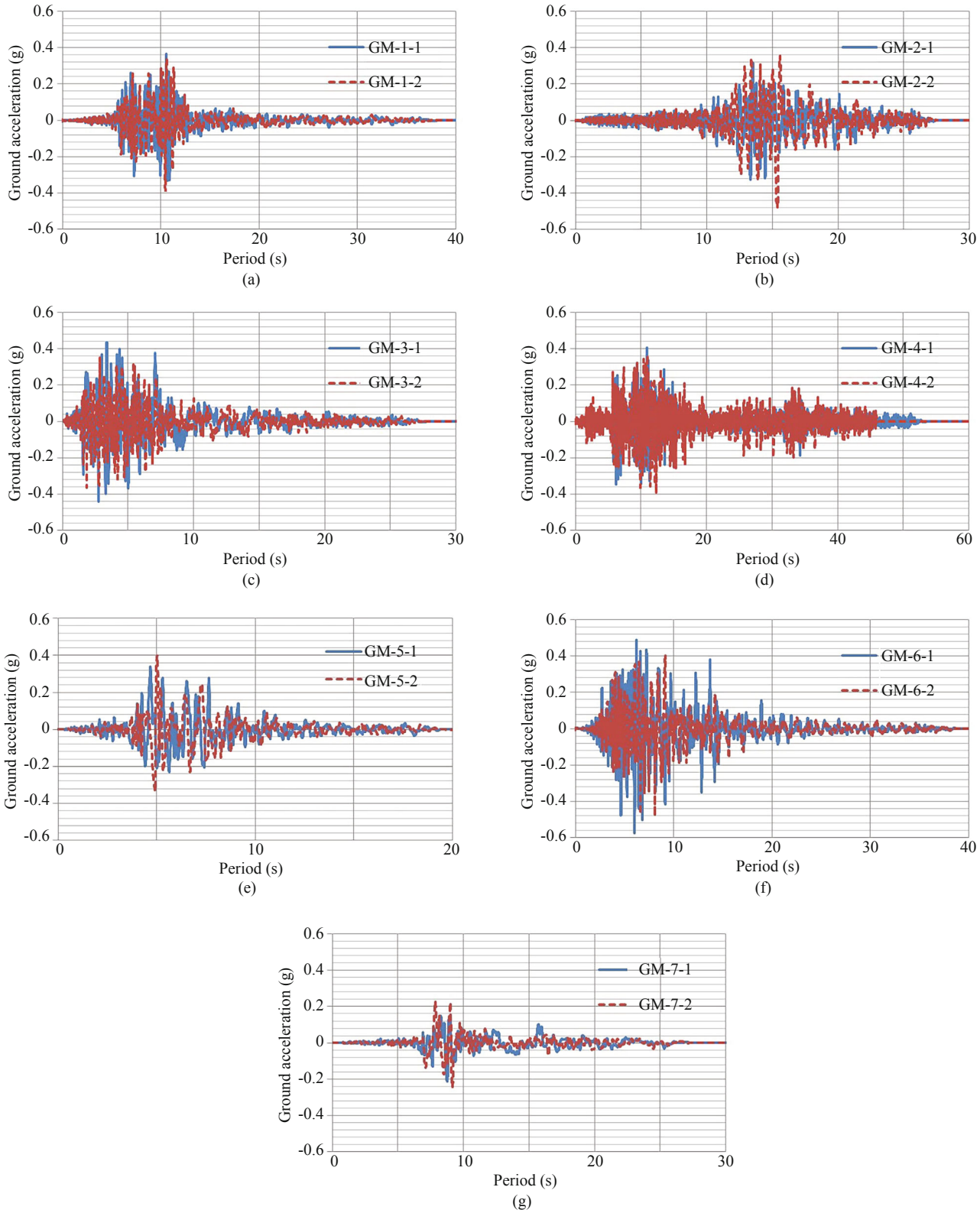

Fig. 11 Seven pairs of ground motions from FEMA-P695 (2009)

the period in the direction of the applied ground motion. This also means that the two ground motions in the same pair were scaled differently, due to the different periods in the longitudinal and transverse direction of the bridge. Since the behavior of the bridge in the longitudinal and transverse direction of the straight bridge is independent from each other, this is a reasonable approach. The scale factors for these ground motions are presented in Table 3, when each component was applied in the bridge's longitudinal and transverse directions

Table 3 Scale factors for the seven pairs of ground motions

	GM 1-1	GM 1-2	GM 2-1	GM 2-2	GM 3-1	GM 3-2	GM 4-1	GM 4-2	GM 5-1	GM 5-2	GM 6-1	GM 6-2	GM 7-1	GM 7-2
L*	0.913	0.986	0.625	0.85	1.071	0.815	0.984	0.906	0.631	0.395	1.007	1.082	0.858	0.87
T*	0.583	0.66	0.54	0.591	0.981	0.679	0.709	0.819	0.815	0.393	0.917	1.508	0.738	0.975

*"L" and "T " stand for "Longitudinal" and "Transverse" directions, respectively

individually.

A total of 14 nonlinear time history analyses were performed using the 7 pairs of scaled ground motions mentioned above. Rayleigh damping was used in the time history analyses considering a damping ratio of 5% of the critical damping at the first and second periods mentioned above. Table 4 shows the maximum forces and displacements of the transverse BRBs obtained from the analyses for the 14 ground motions shown in Table 3, Note that all transverse BRBs have yielded under all these ground motions. The displacements in BRB-T-5 were the largest. Note that, only the responses of the representative BRB in each group in Table 1 are shown here, and the other BRBs in the same category in Table 1 had the same responses. The ductilities of the transverse BRBs are also tabulated in Table 4. The average ductilities obtained are 7.0, 6.1, and 7.4 for BRB-T-1, BRB-T-3, and BRB-T-5, respectively. The average ductilities for these BRBs obtained under the same ground motions at different locations are found to be close. Recall that, using the simple models presented previously, the theoretically calculated ductility of the transverse BRB in the ductile diaphragms design at the middle span was 7.2, which is 18% larger than the average ductility obtained here for BRB-T-3.

Table 5 shows the maximum forces and displacements of the girder stiffener links obtained from the analyses for the 14 ground motions. The displacements of the girder stiffener links are the same as the transverse BRB at the same location. The ductilities of the girder stiffener links are also tabulated, and the average ductilities are 2.4, 2.1, and 2.6 for G1, G-4, and G-7, respectively. Note that the girder stiffener links have larger yield displacements than the transverse BRB as indicated in Table 2. Therefore, the ductilities in Table 5 are different from that in Table 4 for the transverse BRBs. The ductilities values smaller than 1.0 indicate that the girder stiffener links have not yielded at that point.

Table 6 shows the maximum forces and displacements of the longitudinal BRBs obtained from the analyses for the 14 ground motions. Results show that all longitudinal BRBs have yielded. The displacements in BRB-L-1 are the largest. The ductilities of the longitudinal BRBs are also tabulated, and the average ductilities are 13.1, 8.5, and 10.1 for BRB-L-1, BRBL2, and BRB-L-3, respectively. Recall that the theoretically calculated ductility of the longitudinal BRB in the ductile diaphragm design at the end of the middle span was 12.8, which is 26% larger than the average ductility obtained for BRB-L-3.

Table 7 presents the displacements of the points taken along the bridge superstructure as shown in Fig. 12. The name for these points, "S-*i*-*j*", indicates

Table 4 Responses of the transverse BRBs

		BRB-T-1			BRB-T-3			BRB-T-5		
		Max. force (kN)	Max. displ. (mm)	Ductility	Max. force (kN)	Max. displ. (mm)	Ductility	Max. force (kN)	Max. displ. (mm)	Ductility
GM-1	1	132.11	9.68	4.4	132.11	7.70	3.5	132.11	13.13	5.9
	2	132.11	7.42	3.3	132.11	5.66	2.6	132.11	6.50	2.9
GM-2	1	132.11	22.40	10.1	132.11	20.32	9.1	132.11	25.76	11.6
	2	132.11	7.19	3.2	132.11	5.77	2.6	132.11	7.19	3.2
GM-3	1	132.11	5.23	2.4	132.11	3.96	1.8	132.11	6.71	3.0
	2	132.11	28.63	12.9	132.11	26.90	12.1	132.11	23.52	10.6
GM-4	1	132.11	14.40	6.5	132.11	12.62	5.7	132.11	18.39	8.3
	2	132.11	7.75	3.5	132.11	5.72	2.6	132.11	8.08	3.6
GM-5	1	132.11	17.35	7.8	132.11	15.14	6.8	132.11	24.97	11.2
	2	132.11	19.23	8.7	132.11	17.27	7.8	132.11	18.92	8.5
GM-6	1	132.11	5.11	2.3	132.11	3.40	1.5	132.11	9.07	4.1
	2	132.11	31.09	14.0	132.11	28.17	12.7	132.11	31.70	14.3
GM-7	1	132.11	33.40	15.0	132.11	30.76	13.9	132.11	25.48	11.5
	2	132.11	9.93	4.5	132.11	7.65	3.4	132.11	11.71	5.3

Table 5 Responses of the girder stiffener links

		G-1			G-4			G-7		
		Max. force (kN)	Max. displ. (mm)	Ductility	Max. force (kN)	Max. displ. (mm)	Ductility	Max. force (kN)	Max. displ. (mm)	Ductility
GM-1	1	34.70	9.68	1.5	34.70	7.70	1.2	34.70	13.13	2.1
	2	34.70	7.42	1.2	30.69	5.66	0.9	33.81	6.50	1.0
GM-2	1	34.70	22.40	3.5	34.70	20.32	3.2	34.70	25.76	4.0
	2	34.70	7.19	1.1	31.14	5.77	0.9	34.70	7.19	1.1
GM-3	1	28.47	5.23	0.8	21.35	3.96	0.6	34.25	6.71	1.0
	2	34.70	28.63	4.5	34.70	26.90	4.2	34.70	23.52	3.7
GM-4	1	34.70	14.40	2.3	34.70	12.62	2.0	34.70	18.39	2.9
	2	34.70	7.75	1.2	30.69	5.72	0.9	34.70	8.08	1.3
GM-5	1	34.70	17.35	2.7	34.70	15.14	2.4	34.70	24.97	3.9
	2	34.70	19.23	3.0	34.70	17.27	2.7	34.70	18.92	3.0
GM-6	1	27.58	5.11	0.8	18.68	3.40	0.5	34.70	9.07	1.4
	2	34.70	31.09	4.9	34.70	28.17	4.4	34.70	31.70	5.0
GM-7	1	34.70	33.40	5.2	34.70	30.76	4.8	34.70	25.48	4.0
	2	34.70	9.93	1.6	34.70	7.65	1.2	34.70	11.71	1.8

Table 6 Responses of the longitudinal BRBs

		BRB-L-1			BRB-L-2			BRB-L-3		
		Max. force (kN)	Max. displ. (mm)	Ductility	Max. force (kN)	Max. displ. (mm)	Ductility	Max. force (kN)	Max. displ. (mm)	Ductility
GM-1	1	132.11	20.32	7.9	132.11	7.90	4.8	132.11	6.07	3.7
	2	132.11	30.40	11.7	132.11	11.61	7.0	132.11	14.71	8.9
GM-2	1	132.11	16.33	6.3	132.11	3.84	2.3	132.11	3.43	2.1
	2	132.11	80.16	31.0	132.11	43.21	26.1	132.11	36.04	21.8
GM-3	1	132.11	72.44	28.0	132.11	39.90	24.1	132.11	39.34	23.7
	2	132.11	16.15	6.2	132.11	3.02	1.8	132.11	11.48	6.9
GM-4	1	132.11	23.16	8.9	132.11	7.16	4.3	132.11	8.18	4.9
	2	132.11	25.65	9.9	132.11	8.97	5.4	132.11	20.70	12.5
GM-5	1	132.11	46.20	17.8	132.11	22.48	13.6	132.11	22.58	13.6
	2	132.11	40.44	15.6	132.11	10.85	6.5	132.11	18.85	11.4
GM-6	1	132.11	33.15	12.8	132.11	13.61	8.2	132.11	20.62	12.5
	2	132.11	18.52	7.1	132.11	4.39	2.6	132.11	7.85	4.7
GM-7	1	132.11	18.42	7.1	132.11	5.11	3.1	132.11	10.16	6.1
	2	132.11	32.26	12.5	132.11	14.33	8.6	132.11	15.34	9.3

the location of the points. It first labels the spans, as Span-*i*, with "*i*" ranging from "1" to "3". The "L", "R", and "M" labels, substituted for the "*j*" above, indicate whether the points are at the "Left" or "Right" end, or "Middle" of the span, respectively. Since the bridge is symmetric, only displacements for the points on the bridge's left half are presented in Table 7. In the first and second columns in Table 7, the ground motions applied to the bridge model are indicated for the longitudinal and transverse directions, respectively. The maximum transverse displacement of the bridge model occurred in the middle of Span-2 (i.e. point S-2-M in Fig.12), with a corresponding average transverse displacement at point of 22.2 mm (0.875″). Recall that in the transverse pushover analyses, the transverse displacement of the point S-2-M was 4.8 mm (0.189″), when the transverse BRB first yielded. The resulting ductility is 4.63, which is smaller than the theoretically calculated value of 5.4 considered in the design. The maximum longitudinal displacement of the bridge model occurred in Span-1. Note that the

Table 7 Displacements of the multi-span bridge model superstructure (unit: mm)

Longitudinal GM	Transverse GM	S1-L		S1-R		S2-L		S2-M		Bent top	
		Longi.	Trans.	Longi.	Trans.	Longi.	Trans.	Longi.	Trans.	Longi.	Trans.
GM-1-1	GM-1-2	20.32	11.28	20.19	11.43	18.92	17.58	18.92	17.83	9.55	2.57
GM-1-2	GM-1-1	30.40	8.64	30.35	8.89	34.98	9.55	34.93	10.06	10.92	2.24
GM-2-1	GM-2-2	16.33	26.14	16.33	26.11	17.96	32.41	17.93	32.64	9.17	2.64
GM-2-2	GM-2-1	80.16	9.19	80.14	9.09	68.43	10.67	68.40	10.90	12.80	2.36
GM-3-1	GM-3-2	72.44	6.12	72.52	6.71	71.91	9.63	71.83	10.24	11.05	2.13
GM-3-2	GM-3-1	16.15	33.38	16.08	33.76	29.90	29.77	29.92	30.07	11.33	2.67
GM-4-1	GM-4-2	23.19	16.81	23.09	17.12	24.89	23.80	24.94	24.10	10.01	2.57
GM-4-2	GM-4-1	25.65	9.02	25.76	8.84	41.86	11.68	41.78	11.81	10.21	2.36
GM-5-1	GM-5-2	46.18	20.22	46.13	20.09	47.12	31.19	47.17	31.39	11.07	2.77
GM-5-2	GM-5-1	40.44	22.43	40.41	22.48	41.25	24.46	41.25	24.69	10.39	2.57
GM-6-1	GM-6-2	33.15	5.94	33.25	6.20	43.74	12.78	43.87	13.08	10.59	2.21
GM-6-2	GM-6-1	18.52	36.27	18.54	35.28	24.46	39.32	24.46	39.37	9.17	2.79
GM-7-1	GM-7-2	18.42	38.96	18.42	38.33	23.16	32.08	23.11	32.44	10.16	2.79
GM-7-2	GM-7-1	32.26	11.58	32.44	11.33	34.26	16.00	34.09	16.23	10.34	2.46

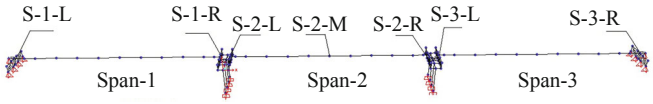

Fig. 12 Locations of the points along the bridge spans where the displacements were monitored

difference of the longitudinal displacements of points S-1-L and S-1-R is negligible, since the axial stiffness of the bridge deck and girders are large. The corresponding average longitudinal displacement at Span-1 is 33.8 (1.332″). The average longitudinal displacement of the middle span (Span-2) is 37.3 mm (1.47″). Recall that in the longitudinal pushover analyses, the longitudinal displacement of the point S2M was 4 mm (0.154″), when the longitudinal BRB first yielded. The resulting ductility is 9.5, which is smaller than the theoretically calculated value of 4.56 as in the design.

In addition to the displacements taken at the level of the bridge deck, the displacements at the top of the bent in both the longitudinal and transverse directions are also tabulated in Table 7. The maximum longitudinal and transverse displacements at the top of the bridge bent are 10.5 mm (0.413″) and 2.5 mm (0.099″), respectively, which are smaller than the bents' yield displacements of 23 mm (0.906″) and 13.2 mm (0.522″) obtained from the pushover analyses. This indicate that the bridge columns remained elastic.

Table 8 shows the total maximum base shear forces obtained from the longitudinal and transverse directions of the multi-span bridge model. The average longitudinal and transverse shear forces obtained from the 14 time history analyses are 1610 kN (362 kips) and 2064 kN (464 kips), respectively. Note that these base shear forces are larger than the maximum forces shown in the pushover analyses, and this is due to the damping forces added to the total base shear forces. Recall that the damping ratio of 5% was considered in the Rayleigh damping setup in the time history analyses. In order to prove this, trial analyses were performed on the bridge model using Rayleigh damping ratio set to zero, and the maximum base shear forces matched exactly with the maximum forces obtained from the pushover analyses. Note that the forces in the BRBs are not affected by this damping ratio.

8 Adding longitudinal BRBs in EDSs

As noticed in Table 6, the longitudinal BRBs in the EDSs (i.e. BRB-L-1) have an average ductility of 13.1. Furthermore, the ductility of the longitudinal BRBs in the ductile diaphragms at the end of the middle span is 26% larger than the average ductility obtained from design calculations. In order to reduce the ductility demand on the longitudinal BRBs in EDSs, the longitudinal stiffness/strength of both EDS in the multispan bridge was doubled by adding another longitudinal BRB, which is the same as BRB-L-1. The effect of this change on the bridge's dynamic behavior in the longitudinal direction was investigated. The EDS at the left end of Span-1 in the new bridge model is shown in Fig. 13. The IDSs stayed the same as in the original bridge model. The longitudinal BRBs in this new bridge model are also categorized into three groups as shown in Table 9.

The longitudinal period of this new bridge model is 0.365 s, which is smaller than the period of 0.41s of the original bridge model (only one longitudinal BRB in the EDSs), and the transverse period stays the same. The

Table 8 Base shear forces of the multi-span bridge model (unit: kN)

Longitudinal GM	Transverse GM	Base shear force	
		Longitudinal	Transverse
GM-1-1	GM-1-2	1459.0	2099.6
GM-1-2	GM-1-1	1636.9	1859.4
GM-2-1	GM-2-2	1432.3	2135.1
GM-2-2	GM-2-1	2046.2	1961.7
GM-3-1	GM-3-2	1730.4	1765.9
GM-3-2	GM-3-1	1445.7	2206.3
GM-4-1	GM-4-2	1530.2	2117.4
GM-4-2	GM-4-1	1574.7	1961.7
GM-5-1	GM-5-2	1690.3	2290.8
GM-5-2	GM-5-1	1685.9	2090.7
GM-6-1	GM-6-2	1645.8	1806.0
GM-6-2	GM-6-1	1454.6	2313.1
GM-7-1	GM-7-2	1556.9	2313.1
GM-7-2	GM-7-1	1654.7	1997.3

Table 9 List of longitudinal BRB groups in the new SAP2000 bridge model

Longitudinal BRB representative member	Location	BRBs with the same response (Location of the BRB)
BRB-L-1	EDS-1	BRB-L-2 (EDS-1) BRB-L-7,8 (EDS-2)
BRB-L-3	IDS-1	BRB-L-6 (IDS-4)
BRB-L-4	IDS-2	BRB-L-5 (IDS-3)

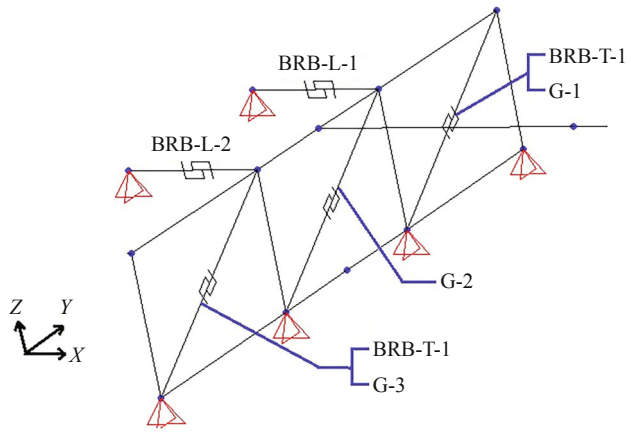

Fig. 13 EDS-1 with two longitudinal BRBs on top of Abutment-1 in the new multi-span bridge model

ground motions were scaled the same way as mentioned earlier, and the scale factors for the ground motions applied to the new bridge model are tabulated in Table 10. Note that scale factors in the transverse direction remained the same as the original bridge model.

Table 11 shows the maximum forces and displacements of the longitudinal BRBs obtained from the analyses for the 14 ground motions. All longitudinal BRBs have yielded. The ductilities of the longitudinal BRBs are also tabulated, and the average ductility is 5.4, 3.0, and 11.1 for BRB-L-1, BRB-L-3, and BRB-L-4, respectively. The displacements in BRB-L-4 in the IDS are the largest. Recall that in the original bridge model, the longitudinal BRB in the EDS had an average ductility of 13.1; here, this ductility demand has been reduced by 59% due to the additional longitudinal BRB in the EDS in the new bridge model. The average ductility demand in the longitudinal BRB in IDS-2 was reduced by 65%. The average ductility demand in the longitudinal BRB in IDS-3 slightly increased, by 10%.

The longitudinal displacement demands were also obtained from the same points as indicated in Fig. 12 along the bridge superstructure. Table 12 shows the longitudinal displacements obtained from the new multispan bridge model subjected to the same 7 pairs of ground motions. The reduction percentages of the longitudinal displacements are compared with the results of the original bridge model. The average reduced longitudinal displacement percentages for end spans and the middle span are 63% and 23%, respectively. The longitudinal displacement at top of the bent was also reduced with an average percentage of 33%.

Table 10 Scale factors for the seven pairs of ground motions in the new bridge model

	GM 1-1	GM 1-2	GM 2-1	GM 2-2	GM 3-1	GM 3-2	GM 4-1	GM 4-2	GM 5-1	GM 5-2	GM 6-1	GM 6-2	GM 7-1	GM 7-2
L*	0.650	0.936	0.5	0.674	1.286	0.6	0.742	0.778	0.586	0.342	0.824	1.051	0.799	0.778
T*	0.583	0.66	0.54	0.591	0.981	0.679	0.709	0.819	0.815	0.393	0.917	1.508	0.738	0.975

*"L" and "T" stand for "Longitudinal" and "Transverse" directions, respectively

Table 11 Scale factors for the seven pairs of ground motions in the new bridge model

		BRB-L-1			BRB-L-2			BRB-L-3		
		Max. force (kN)	Max. displ. (mm)	Ductility	Max. force (kN)	Max. displ. (mm)	Ductility	Max. force (kN)	Max. displ. (mm)	Ductility
GM-1	1	29.7	0.298	2.9	29.7	0.096	1.5	29.7	0.342	5.2
	2	29.7	0.644	6.3	29.7	0.193	3.0	29.7	0.800	12.3
GM-2	1	29.7	0.209	2.1	29.7	0.079	1.2	29.7	0.217	3.3
	2	29.7	1.054	10.3	29.7	0.348	5.3	29.7	0.654	10.0
GM-3	1	29.7	1.810	17.8	29.7	0.903	13.8	29.7	2.411	37.0
	2	29.7	0.219	2.1	29.7	0.078	1.2	29.7	0.350	5.4
GM-4	1	29.7	0.426	4.2	29.7	0.140	2.1	29.7	0.546	8.4
	2	29.7	0.479	4.7	29.7	0.201	3.1	29.7	0.697	10.7
GM-5	1	29.7	0.580	5.7	29.7	0.159	2.4	29.7	1.345	20.6
	2	29.7	0.496	4.9	29.7	0.122	1.9	29.7	0.942	14.4
GM-6	1	29.7	0.519	5.1	29.7	0.098	1.5	29.7	0.751	11.5
	2	29.7	0.237	2.3	29.7	0.060	0.9	29.7	0.226	3.5
GM-7	1	29.7	0.194	1.9	29.7	0.057	0.9	29.7	0.319	4.9
	2	29.7	0.566	5.6	29.7	0.197	3.0	29.7	0.502	7.7

Table 12 Longitudinal displacements of the multi-span bridge model superstructure (unit: mm)

Longitudinal GM	Transverse GM	S1-L		S1-R		S2-L		S2-M		Bent top	
		Longi.	Trans.	Longi.	Trans.	Longi.	Trans.	Longi.	Trans.	Longi.	Trans.
GM-1-1	GM-1-2	7.57	63%	7.62	62%	17.42	8%	17.45	8%	4.85	49%
GM-1-2	GM-1-1	16.36	46%	16.41	46%	38.28	-9%	38.48	-10%	8.92	18%
GM-2-1	GM-2-2	5.31	67%	5.41	67%	10.36	42%	10.34	42%	4.52	51%
GM-2-2	GM-2-1	26.77	67%	26.62	67%	40.16	41%	40.18	41%	10.46	18%
GM-3-1	GM-3-2	16.97	77%	16.89	77%	17.17	76%	17.27	76%	11.25	-2%
GM-3-2	GM-3-1	5.56	66%	5.69	65%	16.08	46%	16.00	46%	4.04	64%
GM-4-1	GM-4-2	10.82	53%	10.82	53%	25.40	-2%	25.53	-2%	6.91	31%
GM-4-2	GM-4-1	12.17	53%	12.29	52%	31.83	24%	31.83	24%	7.19	30%
GM-5-1	GM-5-2	14.73	68%	14.78	68%	58.65	-25%	58.75	-25%	8.33	25%
GM-5-2	GM-5-1	12.60	69%	12.55	69%	40.72	1%	40.77	1%	7.77	25%
GM-6-1	GM-6-2	13.18	60%	13.21	60%	33.76	23%	33.78	23%	8.51	20%
GM-6-2	GM-6-1	6.02	67%	5.97	68%	13.67	44%	13.69	44%	4.37	52%
GM-7-1	GM-7-2	4.93	73%	5.11	72%	16.81	27%	16.74	28%	4.01	60%
GM-7-2	GM-7-1	14.38	55%	14.43	56%	27.64	19%	27.46	19%	8.71	16%

Table 13 shows the total maximum longitudinal base shear forces of the new multi-span bridge model, compared with the longitudinal maximum shear forces of the original bridge model presented in Table 8 (the differences are shown in percentages). The average longitudinal shear force obtained from the 14 time history analyses is 1703.7 kN (383 kips), which is 5% percent larger than the average longitudinal shear forces obtained for the original bridge model in Table 8.

Recall that, in the original bridge model, the longitudinal ductile diaphragms at all the spans were designed to have the same stiffness and strength. In the new bridge model, the longitudinal stiffness and the strength in the EDS was doubled. Based on the above comparisons, it is found that increasing the longitudinal stiffness and strength of the EDSs at the end spans is effective in reducing the displacement demands on the longitudinal BRBs in the end spans, as well as the longitudinal displacement at the bent. However , the average ductility demands in all the longitudinal BRBs in the original bridge model are smaller than in the new one. This is advantageous as it could be argued, from an economic perspective, that it is better to have the ductility demands of all longitudinal BRBs as close as possible (so that similar BRBs can be manufactured). Future studies may further investigate how longitudinal BRBs can be rigorously adjusted to try to achieve that objective.

9 Conclusions

In this paper, the dynamic behavior of a multi-span straight bridge with bidirectional ductile diaphragms was investigated. The responses of both the superstructure and substructure were examined by conducting pushover and nonlinear time history analyses. Using the proposed design methodology, the BRBs designed in the bidirectional ductile diaphragms proved able to develop the expected ductile behaviors, while keep the substructures (columns in the bridge bents) elastic in both directions.

In the transverse direction, the same stiffness and strength of the ductile diaphragms was used in the EDSs and IDSs, and the ductility demands in the transverse BRBs from the dynamic analyses results at different locations were close to the designed ductility. The longitudinal ductile diaphragms were designed to have the same stiffness and strength as the transverse ones. Since the bridge bents are weaker in the longitudinal direction, the ductility demand in the longitudinal BRBs were larger than the transverse ones, as both indicated by the design values and dynamic analyses results. Increasing the stiffness and strength of the longitudinal EDSs on top of the abutment in the end spans can be effective in reducing the longitudinal BRB's ductility in the end spans, as well as the longitudinal displacement demand of the bridge and bent columns. While the work presented here demonstrated feasibility of the concept, future research is needed to investigate the concept more thoroughly in various configurations of multi-span bridges, especially considering multi-span skew bridges. Connections details of BRBs to other structural elements in the bridge also need to be evaluated, particularly if using unconventional connections in bridge applications, such to ensure satisfactory performance of BRBs in the designed ductile diaphragm system. The testing of a scale-model of a complete bridge span with bents is also

Table 13 Base shear forces of the new multi-span bridge model (unit: kN)

Longitudinal GM	Transverse GM	Base shear force	
		Longitudinal	%
GM-1-1	GM-1-2	1361.2	7%
GM-1-2	GM-1-1	1908.3	-17%
GM-2-1	GM-2-2	1361.2	5%
GM-2-2	GM-2-1	2215.2	-8%
GM-3-1	GM-3-2	2295.3	-33%
GM-3-2	GM-3-1	1343.4	7%
GM-4-1	GM-4-2	1659.2	-8%
GM-4-2	GM-4-1	1677.0	-6%
GM-5-1	GM-5-2	1841.6	-9%
GM-5-2	GM-5-1	1757.0	-4%
GM-6-1	GM-6-2	1814.9	-10%
GM-6-2	GM-6-1	1396.7	4%
GM-7-1	GM-7-2	1352.3	13%
GM-7-2	GM-7-1	1846.0	-12%

recommended to verify the predicted dynamic responses of a complete system in which the bidirectional ductile diaphragm system is implemented.

Reference

Alfawakhiri F and Bruneau, M. (2001), "Local Versus Global Ductility Demands in Simple Bridges," *Journal of Structural Engineering*, *ASCE*, **127**(5): 554–560.

American Association of State Highway and Transportation Officials (AASHTO) (2011), *AASHTO Guide Specifications for LRFD Seismic Bridge Design* (*2nd Ed.*), Washington, DC.

Bruneau M, Sarraf M, Zahrai SM and Alfawakhiri F (2002), "Displacement-Based Energy Dissipation Systems for Steel Bridges Diaphragms," *Journal of Constructional Steel Research*, **58**(5-8): 801–817.

Carden LP, Itani AM and Buckle IG (2006a), "Seismic Performance of Steel Girder Bridges with Ductile Cross Frames Using Single Angle X Braces," *Journal of Structural Engineering*, *ASCE*, **132**(3): 329–337.

Carden LP, Itani AM and Buckle IG (2006b), "Seismic Performance of Steel Girder Bridges with Ductile Cross Frames Using Buckling-Restrained Braces," *Journal of Structural Engineering*, *ASCE*, **132**(3): 338–345.

Celik O and Bruneau M (2007), "Seismic Behavior of Bidirectional-Resistant Ductile End Diaphragms with Unbonded Braces in Straight or Skewed Steel Bridges," Technical Report MCEER-07-0003, MCEER, University at Buffalo, Buffalo, NY.

Celik O and Bruneau M (2011), "Skewed Slab-on-Girder Steel Bridge Superstructures with Bidirectional-Ductile End Diaphragms," *Journal of Bridge Engineering*, *ASCE*, **16**(2): 207–218.

Computers & Structures Inc. (2016) *CSI Analysis Reference Manual for SAP2000*, CA.

FEMA P-695 (2009), *Quantification of Building Seismic Performance Factors*, Prepared by Applied Technology Council for the Federal Emergency Management Agency, Washington DC.

SAP2000 Version 16 [Computer software], Computers & Structures. Inc, CA

Sarraf M and Bruneau M (1998a), "Ductile Seismic Retrofit of Steel Deck-Truss Bridges. I: Strategy and Modeling," *Journal of Structural Engineering*, *ASCE*, **124**(11): 1253–1262.

Sarraf M and Bruneau M (1998b), "Ductile Seismic Retrofit of Steel Deck-Truss Bridges. II: Design Applications", *Journal of Structural Engineering*, *ASCE*, **124**(11): 1263–1271.

USGS (2017), *US Seismic Design Mpas*, Retrived from http://earthquake.usgs.gov/designmaps/us/application.php?

Wei X and Bruneau M (2016), "Buckling Restrained Braces Applications for Superstructure and Substructure Protection in Bridges," *Technical Report MCEER-16-0009*, MCEER, University at Buffalo, Buffalo, NY.

Wei X and Bruneau M (2017), "Analytical Investigation of Buckling Restrained Braces Applications in Bidirectional Ductile End Diaphragms for Seismic Performance of Slab-on-Girder Bridge," *Engineering Structures Journal*, **141**: 634–650.

Wei X and Bruneau M (2018). "Experimental Investigation of Buckling Restrained Braces for Bridge Bidirectional Ductile End Diaphragms," *Journal of Structural Engineering*, *ASCE*. (in press)

Zahrai SM and Bruneau M (1998), "Impact of Diaphragms on Seismic Response of Straight Slab-on-Girder Steel Bridges," *Journal of Structural Engineering*, *ASCE*, **124**(8): 938–947.

Zahrai SM and Bruneau M (1999a). "Ductile End-Diaphragms for the Seismic Retrofit of Slab-on-Girder Steel Bridges", *Journal of Structural Engineering*, *ASCE*, **125**(1): 71–80.

Zahrai SM and Bruneau M (1999b), "Cyclic Testing of Ductile End-Diaphragms for Slab-on-Girder Steel Bridges," *Journal of Structural Engineering*, *ASCE*, **125**(9): 987–996.